N-terminal SAP97 isoforms differentially regulate synaptic structure and postsynaptic surface pools of AMPA receptors

Lucy Goodman[1], David Baddeley[1,2], Wojciech Ambroziak[1], Clarissa L. Waites[3], Craig C. Garner[4], Christian Soeller[1,5], Johanna M. Montgomery[1]

1. Department of Physiology and Centre for Brain Research, University of Auckland, New Zealand
2. Department of Cell Biology, Yale School of Medicine, USA
3. Department of Pathology and Cell Biology, Columbia University, USA
4. Charité University, Berlin, Germany
5. Physical and Cell Biology, University of Exeter, UK

Corresponding author:
Johanna M. Montgomery, PhD
Department of Physiology and Centre for Brain Research,
University of Auckland,
Private Bag 92019,
Auckland, New Zealand.
Email: jm.montgomery@auckland.ac.nz

Running Title: SAP97 isoforms differentially alter glutamatergic synapses

Text pages: 32

Figures: 6

Tables: 0

Key words: synapse, glutamate receptors, MAGUK, postsynaptic density, dSTORM

This article has been accepted for publication and undergone full peer review but has not been through the copyediting, typesetting, pagination and proofreading process which may lead to differences between this version and the Version of Record. Please cite this article as an 'Accepted Article', doi: 10.1002/hipo.22723

Abstract

The location and density of postsynaptic AMPA receptors is controlled by scaffolding proteins within the postsynaptic density (PSD). SAP97 is a PSD protein with two N-terminal isoforms, α and β, that have opposing effects on synaptic strength thought to result from differential targeting of AMPA receptors into distinct synaptic versus extrasynaptic locations respectively. In this study we have applied dSTORM super resolution imaging in order to localise the synaptic and extrasynaptic pools of AMPA receptors in neurons expressing α or βSAP97. Unexpectedly, we observed that both α and βSAP97 enhanced the localisation of AMPA receptors at synapses. However, this occurred via different mechanisms: αSAP97 increased PSD size and consequently the number of receptor binding sites, whilst βSAP97 increased synaptic receptor cluster size and surface AMPA receptor density at the PSD edge and surrounding perisynaptic sites without changing PSD size. αSAP97 also strongly enlarged presynaptic active zone protein clusters, consistent with both pre- and postsynaptic enhancement underlying the previously observed αSAP97-induced increase in AMPA receptor-mediated currents. In contrast, βSAP97-expressing neurons increased the proportion of immature filopodia that express higher levels of AMPA receptors, decreased the number of functional presynaptic terminals, and also reduced the size of the dendritic tree and delayed the maturation of mushroom spines. Our data reveal that SAP97 isoforms can specifically regulate surface AMPA receptor nanodomain clusters, with βSAP97 increasing extrasynaptic receptor domains at peri-synaptic and filopodial sites. Moreover, βSAP97 negatively regulates synaptic maturation both structurally and functionally. These data support diverging pre- and postsynaptic roles of SAP97 N-terminal isoforms in synapse maturation and plasticity. As numerous splice isoforms exist in other major PSD proteins (e.g. Shank, PSD95, and SAP102), this alternative splicing may result in individual PSD proteins having divergent functional and structural roles in both physiological and pathophysiological synaptic states.

Introduction

Dynamic changes in the strength of excitatory glutamatergic synaptic transmission are thought to underlie how we learn and adapt to our environment (Bliss and Lomo, 1973; Bliss and Collingridge, 1993; Malinow and Malenka, 2002; Vitureira and Goda, 2013). These changes in synaptic strength can be achieved by altering the density of synaptic α-amino-3-hydroxy-5-methyl-4-isoxazolepropionic acid (AMPA)-type glutamate receptors on the postsynaptic membrane (Lüscher et al., 2000; Shi et al., 2001; Montgomery et al., 2001). AMPA receptor location is also critical for determining synaptic strength as receptors located within the postsynaptic density (PSD) beneath active presynaptic terminals will have direct access to glutamate, whereas those located within the dendritic spine neck, dendritic shaft, or soma, are unlikely to contribute to synaptic transmission. Altering the synaptic versus extrasynaptic location of these surface AMPA receptors is another mechanism that a neuron can employ to increase or decrease its synaptic strength (Borgdorff & Choquet 2002; Tardin et al., 2003; Adesnik et al. 2005; Oh et al. 2006; Bats et al. 2007; Ehlers et al. 2007; Jaskolski et al. 2009; Petrini et al., 2009; Makino and Malinow, 2009; Opazo et al., 2010; Patterson et al., 2010). AMPA receptors are inserted into the membrane at perisynaptic sites located a few hundred nanometres from the PSD, and dynamic movement of AMPA receptors has been observed between perisynaptic and synaptic sites (Borgdorff and Choquet, 2002; Tardin et al., 2003; Heine et al., 2008). AMPA receptors diffuse laterally across the membrane surface to be incorporated into the tightly packed PSD scaffold (Tardin et al., 2003; Adesnik et al. 2005; Gerges et al. 2006; Park et al. 2006; Yudowski, 2007; Makino and Malinow, 2009; Wang et al. 2009; Patterson et al. 2010; Kennedy et al. 2010; Tao-Cheng et al., 2011; Tanaka & Hirano 2012), and can also diffuse away from synapses to undergo internalisation at perisynaptic endocytic zones (Man et al., 2000; Petralia et al., 2003).

Although the number of synaptic glutamate receptors is thought to be controlled by PSD scaffolding proteins such as PSD95 and SAP97 (Montgomery et al., 2004; Nakagawa et al., 2004; Schlüter et al., 2006; Regalado et al., 2006; Waites et al., 2009; Zheng et al., 2011; Li et al., 2011), the mechanisms that trap receptors at synaptic versus extrasynaptic sites are not well understood. Electrophysiological evidence supports the idea that two N-terminal SAP97 isoforms, αSAP97 and βSAP97, can differentially control the distribution of surface glutamate receptors: αSAP97 expression drives an increase in synaptic AMPA receptor-mediated currents consistent with localisation of receptors within the synapse directly beneath the active zone. In contrast, βSAP97 decreases synaptic AMPA receptor-mediated currents but increases total

surface currents, consistent with localisation of receptors outside of the synapse at extrasynaptic locations (Waites et al., 2009; Li et al., 2011). The dominant βSAP97 isoform contains an N-terminal L27 domain, whereas the αSAP97 isoform lacks this domain and instead contains two cysteine residues that can be palmitoylated (Schlüter et al., 2006). These differences in the N-terminal structure also confer the isoforms with different functional properties, whereby αSAP97 is stably associated with postsynaptic structures, while βSAP97 exhibits a more dynamic phenotype (Chetkovich et al., 2002; Nakagawa et al., 2004; Waites et al., 2009).

The localisation of synaptic versus extrasynaptic surface receptor pools is important in determining their potential role and ability to contribute to activity-dependent movement to synaptic sites during changes in synaptic strength. However it is currently unknown where SAP97 isoforms target and localise surface AMPA receptors. The advent of super resolution imaging makes it possible to detect synaptic and extrasynaptic receptor locations (e.g. Dani et al., 2010; Nair et al., 2013). In this study we applied dSTORM super resolution imaging (Rust et al., 2006; van de Linde et al., 2009; Baddeley et al., 2011; Klein et al., 2014) to examine surface pools of AMPA receptors at synaptic and extrasynaptic sites in α- versus βSAP97-expressing neurons. Our data reveal that SAP97 isoforms differentially regulate both surface AMPA receptor nanodomain clusters, and also synaptic maturation and presynaptic function, supporting divergent pre- and postsynaptic roles of SAP97 N-terminal isoforms.

Materials & Methods

Expression constructs

Rat α and βSAP97 sequences containing the alternatively spliced I1b, I3, and I5 inserts and fused at the C-terminus with eGFP were subcloned into the *Xba*I/*Eco*RI backbone of the lentiviral vector pFUGW (Lois et al., 2002) under the control of the Ubiquitin promoter resulting in a ~12kb product (Schlüter et al., 2006; Waites et al., 2009; Li et al., 2011). The full-length βSAP97 insert contains an N-terminal L27 domain, whereas the αSAP97 vector contains an N-terminal 10 amino-acid sequence MDCLCIVTTK. Expression of an eGFP plasmid alone was used as a control (BD Bioscience Clontech). The rat GluA1 sequence was tagged at its N-terminus with the Flag epitope tag sequence DYKDDDDK and subcloned into the pcDNA3 plasmid (Lissin et al., 1998; Cheyne and Montgomery, 2008).

Dissociated hippocampal cell culture

Cell culture procedures were performed using a modified Banker protocol (Goslin et al., 1998; Kaech and Banker, 2006). In brief, hippocampi from P0 Wistar rat pups of either sex were dissociated with the cysteine protease Papain (Worthington Biochemical, #LK003178). Neurons were plated on poly-D-lysine coated coverslips at a density of approximately $1x10^5$cells/ml and maintained at 37°C in 5% CO_2. Neurons were transfected via calcium phosphate precipitation at 9 days *in vitro* (DIV) using our standard protocol employed in previous studies (Montgomery and Cheyne, 2008; Waites et al., 2009; Li et al., 2011). Our previous studies have shown that this transfection method induces modest levels of overexpression of SAP97 isoforms that are comparable to endogenous PSD-95 (Waites et al., 2009). As a further control to quantify overexpression levels, we also performed immunostaining experiments for total SAP97 (Thermo Scientific PA1–741, 1:1000) in transfected versus untransfected neurons and measured the intensity ratios of transfected:untransfected neurons as described in our previous publications (Arons et al., 2012; Arons et al., 2016). Intensity ratios revealed SAP97 levels in the neurons transfected with eGFP-αSAP97 were 1.48 ± 0.16 above untransfected neurons (n=8), and neurons transfected with eGFP-βSAP97 were 1.45 ± 0.18 above untransfected neurons (n=6). This quantification is consistent with our previous work in which immunocytochemical analysis of SAP97 and PSD95 overexpression levels revealed only a modest overexpression of the two SAP97 isoforms with our calcium phosphate precipitation method of transfection (Waites et al., 2009).

Immunocytochemistry and FM4-64 labelling

At DIV12, 3 days after transfection, neurons were immunolabelled for imaging experiments. To image surface glutamate receptors with dSTORM, neurons were live immunolabelled for 20 minutes at 37°C against the extracellular N-terminal FLAG-tagged GluA1 (1:50, mouse, Sigma #F1804) followed by immediate fixation. For immunolabelling of intracellular epitopes for dSTORM and confocal imaging, neurons were fixed for 15 minutes with paraformaldehyde (3.6%, VWR Prolab, #VWRC20909.330), permeabilised in Triton X-100 (0.25%, Sigma, #X-100), and blocked for 1 hour in normal goat serum (3%, In Vitro Tech, #VES1000). To detect presynaptic and postsynaptic protein clusters, neurons were labelled with Bassoon (1:1000, mouse, Sapphire Bioscience #ADI-VAM-PS003-F) and Homer antibodies (1:500, rabbit, Santa Cruz Biotechnology #sc-15321) respectively, overnight at 4°C. To enhance the visible morphology of the transfected dendrite, neurons were labelled with antibodies against the exogenous GFP (1:1000-20,000, chicken, Abcam #ab13970).

Primary antibodies used for dSTORM imaging were detected with secondary antibodies raised in goat and conjugated to Alexa Fluor-680 (1:200, anti-mouse, Invitrogen #A21058) or -750 (1:200, anti-rabbit, Invitrogen #A21039). Primary antibodies for confocal or widefield imaging were detected with secondary antibodies raised in goat and conjugated to Alexa Fluor-568 (1:800, anti-mouse, Invitrogen #A11031; 1:1000, anti-chicken, #A11041) or -647 (1:1000, anti-chicken, Invitrogen #A21449).

FM4-64 labelling of functional presynaptic boutons was performed as previously described (Leal-Ortiz et al., 2008; Waites et al., 2009). Briefly, presynaptic boutons were labelled with FM4–64 dye (10 μM; Molecular Probes) by electrical stimulation (10 Hz, 60 sec). Neurons were then washed for 5 min to remove excess dye, fixed as above and imaged by confocal microscopy.

Confocal imaging and analysis

Coverslips used for confocal imaging were mounted in ProLong Gold (Life Technologies #P10144) and imaged using a Zeiss LSM 710 inverted laser scanning confocal microscope. Overview images (4096 x 4096 pixels) of neuronal morphology were captured with a 40x/1.3NA oil immersion objective lens and a pixel size of 80-90 nm to capture the majority of the dendritic tree. For detailed images of synapses, a 512 x 512 region of dendrite was captured with a 63x/1.4NA oil immersion objective lens. Three channel imaging of Alexa Fluor-488, -568, and -647 fluorophores was achieved with 488 nm argon, 561 nm diode-pumped solid state, and 633

nm Helium-Neon laser excitation respectively. The pinhole aperture was set to 1 airy unit, and gain and offset values were adjusted to optimise the signal for each image. Images were acquired as Z-stacks at 200 nm intervals with sufficient depth to capture the entire neuronal process. Multiple colour channels were acquired sequentially and averaged across four frames at 8 bit-depth.

Confocal image analysis was performed using the open-source software package ImageJ (Schneider et al., 2012). To quantify eGFP-αSAP97 and βSAP97 puncta co-localisation with postsynaptic endogenous Homer, confocal eGFP-SAP97 images were background subtracted and thresholded (Image J, rolling ball radius 100 pixels). The resulting binary masks of eGFP-αSAP97 and βSAP97 puncta were overlaid on the corresponding dSTORM Homer image and the number of eGFP-SAP97 puncta co-localised with Homer puncta were counted. To classify dendritic spine morphology, Z-stacks of eGFP immunolabelling were summed into a single plane and a region of dendrite greater than 25µm in length was selected for analysis. The length of the spine was measured from the tip to the base by tracing the spine using ImageJ's segmented line tool: those longer than 3µm were classified as filopodia, and spines less than 3µm in length and with a head:neck ratio > 1.7 were classified as 'mushroom' spines as described in previous studies (Harris et al., 1992; Gardoni et al., 2012). Spines that did not meet either of these criteria were classified as other spine types (stubby or thin; Harris et al., 1992; Gardoni et al., 2012) and were not analysed further. To quantify the enrichment of SAP97 isoforms in spine versus filopodial structures, eGFP-SAP97 intensity measurements were performed along the length of each dendritic shaft, and the eGFP intensity was then also measured for each filopodia or mushroom spine along this length. The total intensity within each mushroom spine or filopodial structure was then normalised to the intensity in the corresponding dendritic shaft. Comparisons of dendritic tree size were made from single-plane overview images of the GFP antibody fluorescence with the cell soma centred in the image. Images were converted to binary masks, and soma size was estimated using an ellipse that occupied the largest surface area without protruding outside of the neuron. Dendritic size was calculated as the total area of the dendritic tree outside of the soma.

dSTORM imaging and analysis

dSTORM image acquisition and processing was performed as previously described (Baddeley et al., 2011). In brief, dSTORM images were acquired on a modified Nikon TE2000 inverted microscope with a Nikon 60x 1.49NA oil immersion total internal reflection fluorescence (TIRF)

objective. A custom optical path was used to illuminate the sample with a highly inclined beam angle below that required for TIRF microscopy but sufficient to reduce the depth of the excitation plane and thus increase the contrast (Tokunaga et al., 2008).

Dual colour super resolution imaging was achieved using a single 671nm red diode laser (Viasho, #VA-I-N-671, 200-300mW) to excite both infra-red Alexa Fluor-680 and -750 fluorescent dyes. Emission light collected by the objective was separated using a dichroic mirror (Chroma Technology, #Q680LP) and passed through an emission filter (Omega optical, #XF3104-690ALP). Emission from the two infra-red dyes was separated into the 'short' (680-740 nm) and 'long' (740-830 nm) components using a 741 nm-centred dichroic mirror (FF741-Di01, Semrock) placed in the light path between the microscope and the camera. The two channels were focused simultaneously onto two halves of a single 512 x 512 pixel EMCCD camera (Andor IXon, #DV887DCS-BV). Laser illumination position and angle were adjusted as necessary to achieve an approximately 10µm illuminated field of view centred on the camera. Image focus was controlled with a Piezo focusing unit (Physik Intrumente, #P-725). To minimise drift, the objective holder was directly mounted to the microscope stage to minimize movement during image acquisition.

Single molecule fluorescent bursts or "events" were detected and their positions estimated using a 2D fitting algorithm that estimates the parameters of a Gaussian model function. To view and interpret the single molecule events in a more conventional image format, the single molecule localisations were converted to a density map using a jittered delaunay triangulation algorithm (Baddeley et al., 2010). The data was rendered according to the published algorithm as a 32-bit image with 5 nm pixel size and, as described, the pixel intensities scaled linearly with the local density of recorded single molecule events.

Analysis of synaptic cluster size and the number of surface Flag-GluA1 clusters were performed using thresholded binary images. dSTORM images were smoothed with a 2-pixel Gaussian filter, and a threshold was calculated such that 75% of the total intensity in the image was retained within the resulting mask. For analysis of synapses, only those Homer or Bassoon clusters that colocalised with the widefield GFP immunolabelling from the same field of view were included in the analysis. The size of synaptic clusters were compared between synapses pooled across images. The number of Flag-GluA1 clusters ≥ 30 nm^2 were measured using binary dSTORM images of surface receptors (MacGillavry et al., 2013). The number of clusters was normalised to the area of the dendrite measured from the widefield GFP immunolabelling.

The total amount of surface Flag-GluA1 expression was measured using the total number of single-molecule events within the image and was normalised to the area of the dendrite. Similarly, the density of Flag-GluA1 or Homer labelling at synapses was measured by normalising the total amount of labelling to the total pixel sum of all available PSDs within the image, defined by Homer immunolabelling. Both measures are described as the mean number of localizations per μm^2 over an imaging period of 18,000 frames. Although there may be some variability in the efficiency of single molecule photoswitching behaviour (Heilemann et al., 2005), this method has been previously used to compare the relative protein content across different synapses under similar conditions (Dani et al., 2010) and in our previous work the number of single-molecule events from labelling of receptors was directly proportional to another independent measure of the number of receptors (Baddeley et al., 2009).

The location of surface Flag-GluA1 subunits with respect to synapses was measured using a distance transform based algorithm implemented in the PYME software package developed in our laboratories and available at https://bitbucket.org/david_baddeley/python-microscopy. The receptor labelling from each image was binned according to its distance relative to the nearest Homer cluster, where each bin includes data from a distance band 20 nm in width. The analysis was performed up to a maximal distance of 500 nm in all directions from the synaptic edge. The fraction of synaptic labelling refers to the fraction of labelling located inside synapses, i.e. the fraction of events overlapping with the Homer based mask which served as a synaptic marker.

Statistical analysis

Statistical comparisons between normally distributed data were made using a one-way analysis of variance (ANOVA) with Tukey post-hoc comparisons. Data is described in the text as the mean ± standard error of the mean (SEM), and the number of samples (*n*) reflects the number of images. Statistical comparisons between non-parametric data sets were made using the Kruskal-Wallis H Test with post-hoc pairwise comparisons. Non-parametric data is described in the text as the median and the interquartile range between the 25^{th} to the 75^{th} percentile (in the format median/25-75 percentile), and the number of samples is described as X/Y, where Y refers to the number of images from which X synapses were obtained. Significance values (*p*) were set to 0.05 for all analyses and adjusted for multiple comparisons.

Results

To examine the localisation of surface pools of AMPA receptors by α and βSAP97 isoforms we performed dual colour dSTORM imaging on cultured rat hippocampal neurons that expressed either α- or βSAP97-eGFP with Flag-GluA1 (cyan), and immunostained for endogenous Homer (red) to mark postsynaptic densities (PSDs; Fig. 1-3). As previously described, Homer-labelled PSDs were evident as elongated clusters representing synapses from the "side view" and as rounded clusters representing synapses from the "face view" (Dani et al., 2010; Fig. 1, 3, 4). Surface labelling of Flag-GluA1 revealed non-uniform clusters of receptors not only within PSDs, but also over the dendritic and spine surface (Fig. 1A-E, 2A-E, 3A-C, E). Flag-GluA1 clusters located within PSDs likely represent subsynaptic AMPA receptor domains described previously (Ehlers et al., 2007; Heine et al., 2008; Dani et al., 2010; Kerr and Blanpied, 2012; Hoze et al., 2012; MacGillavry et al., 2013). The surface Flag-GluA1 clusters located outside the Homer-labelled PSDs, at non-synaptic sites (Fig. 1A-E, 2A-E), likely reflect extrasynaptic AMPA receptor pools that are thought to contribute to synaptic plasticity through lateral diffusion across the dendritic membrane (Heine et al., 2008; Makino and Malinow, 2009; Patterson et al., 2010; Tao-Cheng et al., 2011). These extrasynaptic receptor clusters were located over the surface of the dendritic membrane, ranging from immediately adjacent to several hundred nanometers away from the closest PSD (Fig. 2).

The total amount of surface Flag-GluA1 labelling (as measured by counting dSTORM single molecule events, see Methods) was not significantly different between neurons expressing eGFP, αSAP97, or βSAP97 (Fig. 1A-D; ANOVA: $F(2, 54) = 0.955$, $p = 0.391$), showing that the overexpression of either SAP97 isoform did not induce changes in the total amount of surface receptor expression. However, αSAP97 and βSAP97 did reduce the total number of Flag-GluA1 surface clusters compared to eGFP controls (Fig. 1E; ANOVA: $F(2, 54) = 21.449$, $p < 0.001$: eGFP: 7.770 ± 0.407 cluster/μm^2; $n = 21$; α: 5.443± 0.340 cluster/μm^2, $n = 18$; $p < 0.001$; β: 4.737 ± 0.259 cluster/μm^2, $n = 18$; $p < 0.001$).

To quantify the radial distribution of surface GluA1 clusters, we measured the location of the Flag-GluA1 labelling relative to immunolabelling for the PSD protein Homer. Receptor labelling that overlapped with Homer-labelled PSDs was characterised as synaptic, whilst labelling located outside PSDs was characterised as extrasynaptic. Compared to eGFP control neurons, both α- and βSAP97 significantly increased the proportion of Flag-GluA1 at synaptic sites and reduced the proportion of receptor labelling located at extrasynaptic sites (Fig. 2A; ANOVA: $F(2, 54) = 33.825$, $p < 0.001$; fraction synaptic labelling: αSAP97 = 0.356 ± 0.019, $n = 18$, $p <$

0.001; βSAP97 = 0.356 ± 0.018, n = 18, p < 0.001; eGFP = 0.204 ± 0.010, n = 21). Analysis of the sub-synaptic receptor clusters revealed differences in morphology, with βSAP97 expression significantly increasing the size of synaptic receptor clusters, whereas αSAP97 expression had no effect (Fig. 2B: K-W test: $X^2(2) = 25.532$, $p < 0.001$; median/lower quartile – upper quartile: α: 0.011/0.004-0.039 μm^2, n = 842/18, p = 1.000; β: 0.019/0.006-0.089 μm^2, n = 482/18, p < 0.001; eGFP: 0.013/0.005-0.038 μm^2; n = 644/21).

We next examined the extrasynaptic surface AMPA receptor pools, as defined by Flag-GluA1 labelling that localised outside of Homer-labelled PSDs. The location of Flag-GluA1 labelling is depicted as distance from the PSD edge in any outward direction up to 500 nm, with the PSD edge at 0 nm (Fig. 2C). In all neurons, receptor clusters in the extrasynaptic pool were more likely to be located close to PSDs, however βSAP97-expressing neurons had the highest fraction of receptor labelling at the PSD edge. The fraction of Flag-GluA1 decreased as the distance from the PSD increased (Fig. 2C). Analysis of the perisynaptic fraction of GluA1, defined as extrasynaptic GluA1 labelling located within 100 nm of the PSD edge, showed that βSAP97 expressing neurons specifically contained a higher proportion of receptor labelling within these perisynaptic sites compared to eGFP controls, whilst αSAP97 has no significant effect (Fig. 2D: ANOVA: F(2, 54) = 10.739, p < 0.001; fraction perisynaptic labelling: α: 0.249 ± 0.010, n = 18, p = 0.123; β: 0.285 ± 0.012, n = 18, p < 0.001; eGFP: 0.222 ± 0.006, n = 21). The size distribution of GluA1 receptor clusters revealed that extrasynaptic receptor clusters were smaller than synaptic receptor clusters (compare Fig. 2B and E). Consistent with their increased synaptic receptor localisation, both α and βSAP97 expression reduced the size of extrasynaptic receptor clusters (Fig. 2E: K-W test: $X^2(2) = 50.936$, $p < 0.001$; median/lower quartile – upper quartile: α: 0.005/0.003-0.010 μm^2, n = 2283/18, p < 0.001; β: 0.006/0.003-0.011 μm^2, n = 2022/18, p < 0.001; eGFP: 0.007/0.003-0.014 μm^2; n = 2479/21). Overall, these data show isoform-dependent regulation of surface AMPA receptor distribution in synaptic and extrasynaptic nanodomains.

Changes in surface AMPA receptor distribution may also reflect changes in other PSD proteins (MacGillavry et al., 2013; Nair et al., 2013; Fukata et al., 2013). We therefore next focussed on the Homer-labelled PSDs in α- and βSAP97 expressing neurons. Both αSAP97 and βSAP97 eGFP puncta highly co-localised with endogenous Homer clusters (αSAP97: 92.067 ± 2.535%; βSAP97: 93.058 ± 1.678%; n = 18), consistent with our previous confocal imaging data showing both isoforms localise at postsynapses (Waites et al., 2009). dSTORM imaging of endogenous Homer labelling revealed elongated PSD structures in the “side view” and more spherical disk

shapes in the "face" views (Fig. 3A-F; Dani et al., 2010). The size of the Homer-labelled PSDs was significantly increased in αSAP97 expressing neurons compared to eGFP controls, whereas βSAP97 had no significant effect (Fig. 3D; K-W test: $X^2(2) = 9.690$, $p = 0.008$; α = 0.090/0.054-0.190μm^2, $n = 392/18$, $p = 0.006$; β = 0.081/0.054-0.156 μm^2, $n = 310/18$, $p = 0.251$; eGFP = 0.078/0.053-0.121μm^2, $n = 323/24$). To determine whether this increase in PSD size in αSAP97 neurons is sufficient to explain the observed increase in the fraction of synaptic GluA1 receptor clusters, we measured the density of single-molecule localisations of Flag-GluA1 labelling per μm^2 of Homer-labelled PSD, as a proxy for synaptic receptor labelling density. The density of synaptic receptors in PSDs from αSAP97-expressing neurons was not statistically different to the density in eGFP controls (Fig. 3E; ANOVA: $F(2, 54) = 9.879$, $p < 0.001$; α = 57.791 ± 5.270 localizations/μm^2, $p = 0.231$; eGFP = 44.918 ± 5.734 localizations/μm^2), indicating that αSAP97 increases the number of receptors at synapses in proportion to the PSD size. In contrast, βSAP97 expressing neurons contained a significantly higher density of synaptic Flag-GluA1 labelling (β = 79.271 ± 5.499 localizations/μm^2, $p < 0.001$). No changes were observed in the density of Homer PSD labelling from the same population of synapses in αSAP97, βSAP97, and eGFP-expressing neurons (Fig. 3F; ANOVA: $F(2, 54) = 0.077$, $p = 0.926$). Together, this evidence suggests that αSAP97 promotes AMPA receptor incorporation into synapses by increasing the size of the PSD and therefore the number of receptor binding sites, whereas βSAP97 acts to promote AMPA receptor incorporation into synapses independently of the size of the synapse.

The increased PSD size and consequently the amount of AMPA receptors in αSAP97-expressing neurons likely underlies the increased AMPA receptor mediated synaptic current amplitudes previously observed in these neurons (Waites et al., 2009; Li et al., 2011). To confirm that these large αSAP97 expressing PSDs are associated with presynaptic active zones, we performed dSTORM imaging of endogenous presynaptic Bassoon and postsynaptic Homer to neurons expressing αSAP97, βSAP97, or eGFP. Bassoon and Homer protein distributions were evident as juxtaposed pairs of structures in the "side view" separated by the synaptic cleft (Fig. 4; Dani et al., 2010). Synapses were defined as closely opposed Bassoon (presynaptic active zone) and Homer (PSD) structures (Fig. 4A-C; Dani et al., 2010).

Both α and βSAP97 significantly increased the size of Bassoon-labelled structures compared to eGFP controls (Fig. 4D; K-W test: ($X^2(2) = 35.637$, $p < 0.001$; median/lower quartile – upper quartile: α = 0.125/0.069-0.236μm^2, $n = 374/23$, $p < 0.001$; β = 0.103/0.064-0.172 μm^2, $n = 254/17$, $p = 0.001$; eGFP = 0.082/0.061-0.132μm^2, $n = 218/16$). In addition, presynaptic Bassoon labelled structures forming onto αSAP97 expressing neurons were significantly larger than those

forming onto βSAP97-expressing neurons ($p < 0.01$), suggesting that αSAP97 has a dominant ability to alter presynaptic structure. Therefore, although both SAP97 isoforms appear to have the ability to alter the presynapse, αSAP97 more strongly enhances presynaptic active zone protein cluster size, potentially providing postsynaptic AMPA receptors on αSAP97-expressing neurons with increased access to presynaptic glutamate.

The increased clustering of synaptic AMPA receptors in βSAP97-expressing neurons, and the increased size of their presynaptic Bassoon-labelled structures is at odds with the previously observed reduction in AMPA receptor synaptic currents that was measured with paired whole cell recordings (Waites et al., 2009; Li et al., 2011). In addition to postsynaptic receptor localisation and expression levels, other major determinants of AMPA receptor EPSC amplitude include presynaptic transmitter release, synaptic density, synaptic maturation and morphology. Previous studies have shown that postsynaptic density proteins including SAP97 can alter presynaptic structure and function (e.g. Rumbaugh et al., 2003; Regalado et al., 2006; Arons et al., 2012). We therefore performed FM4-64 labelling in α- and βSAP97 expressing neurons to determine whether changes in presynaptic function could contribute to the observed depression in AMPA EPSC amplitude. Analysis of postsynaptic α- and β-SAP97 revealed that significantly fewer βSAP97 puncta co-localise with FM4-64 (Fig. 4E; αSAP97 76.09 ± 3.22; βSAP97 56.34 ± 6.03; $p = 0.017$), suggesting that fewer βSAP97 puncta oppose functional presynaptic terminals.

We also examined whether differences in neuronal and synaptic structure may contribute to the previously observed reduction in glutamatergic synaptic transmission (Waites et al., 2009; Li et al., 2011). We applied confocal imaging to examine neuronal and synaptic morphology as it provides extended fields of view suitable to capture large portions of the dendritic trees (Fig. 5A-C). α- and βSAP97 expressing neurons both exhibit bright punctate expression at synapses (Fig. 5A,B), as previously described (Waites et al., 2009). The total surface area of the dendrites was reduced in βSAP97-expressing but not αSAP97-expressing neurons (Fig. 5D; ANOVA: $F(2, 74) = 12.019$, $p < 0.001$; α = 1904.194 ± 170.934μm^2, $n = 24$, $p = 0.881$: β = 1088.187 ± 63.913μm^2, $n = 23$, $p < 0.001$; eGFP = 1820.792 ± 114.992μm^2, $n = 30$). We also quantified postsynaptic spine morphology to determine the relative frequency of mature mushroom-shaped spines versus developing filopodia based on their length, and the ratio between their head and neck widths (see Methods). βSAP97-expressing neurons were found to possess significantly fewer mushroom-shaped spines compared to eGFP controls and αSAP97-expressing neurons (Fig. 5E; ANOVA:

F(2, 120) = 10.917, $p < 0.001$; α = 20.713 ± 2.528%, $n = 24$, $p = 0.290$: β = 11.168 ± 1.95%, $n = 38$, $p < 0.001$; eGFP = 26.355 ± 2.687%, $n = 43$). βSAP97 neurons also contained a significantly larger proportion of filopodia compared with neurons expressing αSAP97 (Fig. 5F; ANOVA: F(2, 102) = 13.731, $p < 0.001$; α = 12.939 ± 2.478%, $n = 24$, $p = 0.922$: β = 28.625 ± 3.462%, $n = 38$, $p < 0.001$; eGFP = 11.403 ± 1.651%, $n = 43$). To gauge the relative enrichment or localisation of SAP97 isoforms in mushroom spines versus filopodia, we performed intensity measures of eGFP-αSAP97 and eGFP-βSAP97 within mushroom spines and filopodial structures. βSAP97-positive mushroom spines showed similar intensity measurements to αSAP97-positive mushroom spines (intensity ratio of mushroom spine/shaft: α = 0.184 ± 0.039, $n = 24$; β = 0.229 ± 0.066, $n = 29$, $p > 0.05$; data not shown), suggesting that once mature, these synapse types express both SAP97 isoforms at similar levels. However, βSAP97 intensity measurements were significantly higher in the filopodia (α = 0.314 ± 0.053, $n = 24$; β = 0.579 ± 0.088, $n = 29$, $p < 0.05$; data not shown), suggesting an enrichment of this isoform in the more immature filopodial structures.

To determine whether the βSAP97-induced changes in dendritic spine phenotype were due to a slowing of dendritic spine maturation rate or an active prevention of spine formation, we repeated the filopodia/mushroom spine analysis at 21 DIV. At this later stage, we observed that the relative frequency of filopodia was no longer significantly different between α- versus βSAP97 expressing neurons (Fig. 5F; α = 12.875 ± 2.882%, $n = 20$, β = 19.921 ± 4.052%, $n = 18$; $p = 0.159$). However, the frequency of mushroom spines was still significantly higher in αSAP97-expressing neurons at 21 DIV compared with βSAP97 (Fig. 5E; α = 41.976 ± 4.513%, $n = 20$, β = 20.222 ± 3.739%, $n = 18$; $p = 0.001$). Further analyses revealed that βSAP97-expressing neurons showed a higher relative frequency of other spine types, i.e. stubby and thin (Harris et al., 1992; Gardoni et al., 2012), at 21 DIV (α = 45.149 ± 3.767%, $n = 20$, β = 59.858 ± 4.989%, $n = 18$, $p < 0.05$; data not shown). Together these data suggest that βSAP97 alters the balance of dendritic spines towards those with a more immature phenotype by delaying the maturation of filopodia, and that by 3 weeks in vitro the filopodia have begun maturation into other spine types.

Previous electrophysiology studies detected a large population of extrasynaptic AMPA receptors in βSAP97-expressing neurons as evidenced by a significant increase in the response to exogenously applied AMPA to the neuron surface (Waites et al., 2009; Li et al., 2011). To investigate whether the large population of filopodia on βSAP97-expressing neurons are a source

of extrasynaptic receptors, we performed dSTORM imaging of surface Flag-GluA1 on filopodia identified by widefield eGFP fluorescence from the same field of view. Flag-GluA1 clusters were consistently observed along the surface of filopodia in control neurons (eGFP) and in neurons expressing αSAP97 or βSAP97 (Fig. 6A-C). Quantification of the area of Flag-GluA1 clusters on the filopodial surface revealed a significant increase in Flag-GluA1 on filopodia in βSAP97-expressing neurons (Fig. 6D; ANOVA: $F(2, 58) = 8.557$, $p = 0.001$; α = 0.171 ± 0.034μm^2, $n = 17/11$, $p = 0.972$; β = 0.499 ± 0.076 μm^2, $n = 28/18$, $p = 0.005$; eGFP = 0.195 ± 0.046 μm^2, $n = 16/11$). These data show that a significant proportion of surface extrasynaptic AMPA receptors are localised on the immature filopodia that occur in higher frequency in βSAP97-expressing neurons.

Discussion

In this study we performed dSTORM super resolution imaging (Rust et al., 2006; van de Linde et al., 2009; Baddeley et al., 2011; Klein et al., 2014) to examine surface pools of AMPA receptors. Our previous electrophysiological data were consistent with αSAP97 localising receptors to synapses, and with βSAP97 localising receptors to extrasynaptic sites (Waites et al., 2009; Li et al., 2011). Therefore we reasoned that these SAP97 isoforms could provide us with a way to examine the localisation and distribution of synaptic versus extrasynaptic AMPA receptors. dSTORM imaging of surface AMPA receptor distribution revealed that expression of SAP97 isoforms did not alter the total amount of surface receptor expression. However, SAP97 isoforms did decrease the number of surface receptor clusters, consistent with these scaffold proteins driving surface receptors into distinct domains. Surprisingly, our data reveal that both αSAP97 and βSAP97 significantly increase AMPA receptor expression within the PSD. However, this resulted from different mechanisms as αSAP97 increases synaptic receptors by increasing PSD size, whereas βSAP97 increases synaptic receptor cluster size, as well as receptor density at the PSD edge and surrounding perisynaptic sites. βSAP97 is more highly expressed in filopodia where it drives higher AMPA receptor expression at extrasynaptic filopodial sites, and decreases the frequency of functional mature synapses by delaying their maturation. In contrast, αSAP97 drives synapses into a mature state, increasing the frequency of functional synapses. Our data show that the previously observed differences in synapse physiology between α and βSAP97 neurons result not only from differential localisation of surface synaptic and extrasynaptic AMPA receptors, but also from changes in synaptic structure and maturation that occur at both presynaptic and postsynaptic sites.

To date, super resolution imaging of AMPA receptors has largely focussed on synaptic receptors, revealing they are organised in nanodomains within the PSD where they co-localise with PSD scaffold clusters (Grunwald et al., 2011; MacGillavry et al., 2013; Nair et al., 2013; Szepesi et al., 2014; Jacob and Weinberg, 2015). We observed that βSAP97 selectively drives an increase in the size of receptor clusters at synapses, suggesting that SAP97 isoforms can specifically regulate distinct subsynaptic nanodomains of AMPA receptors. In addition to synaptic AMPA receptor nanodomains, we also observed clusters of AMPA receptors at perisynaptic and extrasynaptic sites. The majority of the extrasynaptic receptor clusters were located in the perisynaptic region within 100 nm of the PSD edge, where glutamate receptors are proposed to undergo endocytosis (Blanpied et al., 2002), and where exchange between synaptic and

extrasynaptic sites is likely controlled. These extrasynaptic receptor clusters are smaller than synaptic clusters, which likely results from the significant decrease in receptor scaffold proteins in this region, enabling them to disperse across the membrane and exhibit high mobility (Tardin et al., 2003).

With regards to synaptic AMPA receptor pools, i.e. those that localised within Homer-labelled PSDs, our data suggest that αSAP97 increased the numbers of synaptic receptors by increasing PSD size and therefore the number of receptor binding sites. Previous biochemical data have shown a tighter association of αSAP97 with the lipids and proteins of the PSD than βSAP97 (Waites et al., 2009). The higher relative levels of βSAP97 measured in immature filopodia that lack mature PSDs likely contributes this isoform-specific difference in PSD association. αSAP97's palmitoylated cysteine residues have been proposed to be critical for targeting and anchoring αSAP97 to the mature PSD (Waites et al., 2009), and palmitoylation of PSD proteins has been shown to regulate AMPA receptor trafficking and accumulation at the postsynapse (deSouza and Ziff, 2002). Palmitoylation of αPSD95 induces the formation of subsynaptic clusters that contain AMPA receptors, and a higher number of αPSD95 clusters correlates with increased postsynaptic size (Fukata et al., 2013). As αSAP97 shares nearly identical N-terminal sequences and palmitoylation of N-terminal cysteines with αPSD95 (Craven et al., 1999; El-Husseini et al., 2000; Montgomery et al., 2004; Schluter et al., 2006; Waites et al., 2009), and can rescue AMPA receptor-mediated synaptic transmission following loss of PSD95 (Schluter et al., 2006; Waites et al., 2009), significant functional redundancy may occur between these two proteins within mature PSDs. αSAP97 may therefore perform a role similar to that of αPSD95 to increase the synaptic AMPA receptor scaffolding abilities at synapses (Liu et al., 2014). We hypothesise that palmitoylation contributes to the ability of αSAP97 to increase synaptic AMPA receptor scaffolding and mature mushroom spines in proportion with the increased size of the PSD, promoting existing surface receptors into synapses by increasing the number of receptor binding sites or receptor nanodomains in a similar fashion to αPSD95.

Electrophysiological studies of the effects of βSAP97 on glutamatergic synaptic transmission have produced conflicting results as βSAP97 has been shown to increase (Rumbaugh and Sia, 2003; Nakagawa et al., 2004; Schlüter et al., 2006; Howard et al., 2010; Liu et al., 2014), decrease (Waites et al., 2009; Li et al., 2011), or not alter (Schnell et al., 2002; Rumbaugh and Sia, 2003; Howard et al., 2010) AMPA receptor-mediated transmission. These conflicts may reflect the difficulty in assigning a single function to a protein with multiple sites of alternative

splicing, and the use of variable or unstated βSAP97 splice variants makes comparisons between studies difficult. Nonetheless, by significantly increasing the resolution of surface receptor localisation our dSTORM analyses of α- and βSAP97 expressing synapses reveals that βSAP97 can induce an approximately two-fold increase in synaptic GluA1 density and cluster size without any significant changes to PSD size. This suggests that βSAP97 can also promote AMPA receptor movement into synapses from perisynaptic and extrasynaptic regions and act as a molecular scaffold for AMPA receptors at synapses.

This βSAP97-induced increase in synaptic receptors initially appeared in contradiction to our previously observed decrease in synaptic current amplitude (Waites et al., 2009; Li et al., 2011). However, super-resolution imaging revealed that βSAP97 also localises AMPA receptors at the PSD edge and in perisynaptic regions. Localisation of synaptic βSAP97-bound AMPA receptor clusters at the edges of the PSD could contribute to the inability of these receptors to detect synaptically released glutamate, especially if presynaptic function is also compromised, and consequently increasing the odds of "off cluster" events occurring (MacGillavry et al., 2013). Conversely, αSAP97 may optimise synaptic receptor cluster positioning for detection of synaptic released glutamate. Our STORM data are consistent with previous electron microscopy studies which have shown that SAP97 and GluA1 concentrate at the edge of the PSD and extend into extrasynaptic regions (DeGiorgis et al., 2006; Waites et al., 2009; Jacob and Weinberg, 2015). While it is not stated which isoform(s) were detected in two of these studies (deGiorgis et al., Jacob and Weinberg), both examined endogenous SAP97, which is predominantly βSAP97 (Rumbaugh et al., 2003; Schluter et al., 2006; Waites et al., 2009; Li et al., 2011). However, our previous electron microscopy imaging showed that βSAP97 was localised more towards peri-synaptic sites (Waites et al., 2009). Together these data suggest a role of βSAP97 in stabilising receptor clusters at the edge of the PSD, and therefore may regulate the movement of receptors from extrasynaptic to synaptic pools.

Another major difference between α- and βSAP97 expressing neurons is that βSAP97 does not drive a parallel increase in presynaptic function. Previous work has shown that SAP97 can drive trans-synaptic increases in presynaptic protein expression (Regalado et al., 2006), however which isoform induced these changes, and the frequency of these larger synapses was not specified. We observed that βSAP97 can also increase presynaptic Bassoon, consistent with this previous study, although it was not to the same extent as αSAP97. Our data are consistent with SAP97 being a major driver to trans-synaptically alter presynaptic structure and function, as well

as postsynaptic maturation. Intriguingly, βSAP97 influences presynaptic function in the negative direction, with FM4-64 labelling showing a reduced number of functional presynaptic terminals. βSAP97 is also highly expressed in immature filopodial structures, and consequently limited neuronal maturation, driving a significant increase in the frequency of immature filopodia, a decrease in mature mushroom spines, and an approximate halving of the area of the dendritic tree. Together, these likely result in weaker synaptic strength and decreased synaptic stability of βSAP97 (Waites et al., 2009; Li et al., 2011). Therefore, the increase in synaptic receptors induced by βSAP97 may compensate for decreased presynaptic function and postsynaptic maturation. The increase in extrasynaptic receptors localised on dendritic filopodia are likely the source of extrasynaptic receptors previously detected with electrophysiology (Waites et al., 2009; Li et al., 2011). The localisation of these extrasynaptic receptors on filopodia could also explain why this extrasynaptic receptor pool does not appear to contribute to LTP (Li et al., 2011).

In summary, our data show that the divergent functional changes in synaptic transmission induced by N-terminal isoforms of SAP97 result from differential receptor cluster localisation and maturation of pre- and postsynaptic structures. These data reveal that splice isoforms within one PSD protein can induce distinctly different functional and structural changes, and therefore that one protein can have divergent roles at excitatory synapses. Splice isoforms exist for many PSD proteins in addition to SAP97, including PSD95, Shanks 1-3, SAP102 and PSD93 to name just a few. As such, determining whether each isoform plays a different functional role is critical to understanding why so many isoforms exist, and also whether their potentially divergent roles could be utilised in physiological and pathophysiological states.

References

Adesnik H, Nicoll RA, England PM. 2005. Photoinactivation of native AMPA receptors reveals their real-time trafficking. Neuron 48:977–85.

Arons MH, Thynne CJ, Grabrucker AM, Li D, Schoen M, Cheyne JE, Boeckers T, Montgomery JM, Garner CC. 2012. Autism-associated mutations in ProSAP2/Shank3 impair synaptic transmission and neurexin-neuroligin-mediated transsynaptic signaling. J Neurosci 32:14966-14978.

Baddeley D, Jayasinghe ID, Lam L, Rossberger S, Cannell MB, Soeller C. 2009. Optical single-channel resolution imaging of the ryanodine receptor distribution in rat cardiac myocytes. Proc Natl Acad Sci 106:22275-22280.

Baddeley D, Cannell MB, Soeller C. 2010. Visualization of localization microscopy data. Microsc Microanal 16:64–72.

Baddeley D, Crossman D, Rossberger S, Cheyne JE, Montgomery JM, Jayasinghe ID, Cremer C, Cannell MB, Soeller C. 2011. 4D super-resolution microscopy with conventional fluorophores and single wavelength excitation in optically thick cells and tissues. PLoS One 6.

Bats C, Groc L, Choquet D. 2007. The interaction between Stargazin and PSD-95 regulates AMPA receptor surface trafficking. Neuron 53:719–34.

Blanpied TA, Scott DB, Ehlers MD. 2002. Dynamics and regulation of clathrin coats at specialized endocytic zones of dendrites and spines. Neuron 36:435–49.

Bliss TVP, Lømo T. 1973. Long-lasting potentiation of synaptic transmission in the dentate area of the anaesthetized rabbit following stimulation of the perforant path. J Physiol 232:331-356.

Bliss TVP, Collingridge GL. 1993. A synaptic model of memory: long-term potentiation in the hippocampus. Nature 361:31–39.

Borgdorff AJ, Choquet D. 2002. Regulation of AMPA receptor lateral movements. Nature 417:649–653.

Buss F, Arden SD, Lindsay M, Luzio JP, Kendrick-Jones J. 2001. Myosin VI isoform localized to clathrin-coated vesicles with a role in clathrin-mediated endocytosis. EMBO J 20:3676–3684.

Chen L, Chetkovich DM, Petralia RS, Sweeney NT, Kawasaki Y, Wenthold RJ, Bredt DS, Nicoll RA. 2000. Stargazin regulates synaptic targeting of AMPA receptors by two distinct mechanisms. Nature 408:936–943.

Chetkovich DM, Bunn RC, Kuo SH, Kawasaki Y, Kohwi M, Bredt DS. 2002. Postsynaptic targeting of alternative postsynaptic density-95 isoforms by distinct mechanisms. J Neurosci 22:6415–25.

Cheyne JE, Montgomery JM. 2008. Plasticity-dependent changes in metabotropic glutamate receptor expression at excitatory hippocampal synapses. Mol Cell Neurosci 37:432–439.

Craven SE, El-Husseini AE, Bredt DS. 1999. Synaptic targeting of the postsynaptic density protein PSD-95 mediated by lipid and protein motifs. Neuron 22:497–509.

Dani A, Huang B, Bergan J, Dulac C, Zhuang X. 2010. Superresolution imaging of chemical synapses in the brain. Neuron 68:843–856.

DeGiorgis JA, Galbraith JA, Dosemeci A, Chen X, Reese TS. 2006. Distribution of the scaffolding proteins PSD-95, PSD-93, and SAP97 in isolated PSDs. Brain Cell Biol 35:239-50.

deSouza S, Ziff EB. 2002. AMPA receptors do the electric slide. Science's STKE 156:45.

Ehlers MD, Heine M, Groc L, Lee MC, Choquet D. 2007. Diffusional trapping of GluR1 AMPA receptors by input-specific synaptic activity. Neuron 54:447-60.

El-Husseini AE, Craven SE, Chetkovich DM, Firestein BL, Schnell E, Aoki C, Bredt DS. 2000. Dual palmitoylation of PSD-95 mediates its vesiculotubular sorting, postsynaptic targeting, and ion channel clustering. J Cell Biol 148:159–172.

Fiala JC, Feinberg M, Popov V, Harris KM. 1998. Synaptogenesis via dendritic filopodia in developing hippocampal area CA1. J Neurosci 18:8900–8911.

Fukata Y, Dimitrov A, Boncompain G, Vielemeyer O, Perez F, Fukata M. 2013. Local palmitoylation cycles define activity-regulated postsynaptic subdomains. J Cell Biol 202:145–161.

Gardoni F, Mauceri D, Fiorentini C, Bellone C, Missale C, Cattabeni F, Di Luca M. 2003. CaMKII-dependent phosphorylation regulates SAP97/NR2A interaction. J Biol Chem 278:44745–44752.

Gardoni F, Saraceno C, Malinverno M, Marcello E, Verpelli C, Sala C, Di Luca M. 2012. The neuropeptide PACAP38 induces dendritic spine remodeling through ADAM10-N-cadherin signaling pathway. J Cell Sci 125:1401-1406.

Gerges NZ, Backos DS, Rupasinghe CN, Spaller MR, Esteban JA. 2006. Dual role of the exocyst in AMPA receptor targeting and insertion into the postsynaptic membrane. EMBO Journal 25:1623–34.

Goslin K, Asmussen H, Banker G. 1998. Rat hippocampal neurons in low-density culture. In: Banker G, Goslin K, editors. Culturing nerve cells, Second edition. MIT Press. p 339-370.

Grunwald C, Schulze K, Giannone G, Cognet L, Lounis B, Choquet D, Tampé R. 2011. Quantum-yield-optimized fluorophores for site-specific labeling and super-resolution imaging. J Am Chem Soc 133:8090-3.

Harris KM, Jensen FE, Tsao B. 1992. Three-dimensional structure of dendritic spines and synapses in rat hippocampus (CA1) at postnatal day 15 and adult ages: implications for the maturation of synaptic physiology and long-term potentiation. J Neurosci 12:2685–2705.

Heilemann M, Margeat E, Kasper R, Sauer M, Tinnefeld P. 2005. Carbocyanine dyes as efficient reversible single-molecule optical switch. J Am Chem Soc 127:3801–3806.

Heine M, Groc L, Frischknecht R, Bé J, Lounis B, Rumbaugh G, Huganir RL, Cognet L, Choquet D. 2008. Surface Mobility of Postsynaptic AMPARs Tunes Synaptic Transmission. Science 320:201-5.

Howard MA, Elias GM, Elias LB, Swat W, Nicoll RA. 2010. The role of SAP97 in synaptic glutamate receptor dynamics. Proc Natl Acad Sci 107:3805–3810.

Hoze N, Nair D, Hosy E, Sieben C, Manley S, Herrmann A, Sibarita JB, Choquet D, Holcman D. 2012. Heterogeneity of AMPA receptor trafficking and molecular interactions revealed by superresolution analysis of live cell imaging. Proc Natl Acad Sci 109:17052–7.

Jacob AL, Weinberg RJ. 2015. The organization of AMPA receptor subunits at the postsynaptic membrane. Hippocampus 25:798-812.

Jaskolski F, Mayo-Martin B, Jane DE, Henley JM. 2009. Dynamin-dependent membrane drift recruits AMPA receptors to dendritic spines. J Biol Chem 284:12491–503.

Jeyifous O, Waites CL, Specht CG, Fujisawa S, Schubert M, Lin EI, Marshall J, Aoki C, De Silva T, Montgomery JM, Garner CC, Green WN. 2009. SAP97 and CASK mediate sorting of NMDA receptors through a previously unknown secretory pathway. Nat Neurosci 12:1011–1019.

Kaech S, Banker G. 2006. Culturing hippocampal neurons. Nat Protoc 1:2406–2415.

Kennedy MJ, Davison IG, Robinson CG, Ehlers MD. 2010. Syntaxin-4 defines a domain for activity-dependent exocytosis in dendritic spines. Cell 141:524–35.

Kerr JM, Blanpied TA. 2012. Subsynaptic AMPA receptor distribution is acutely regulated by actin-driven reorganization of the postsynaptic density. J Neurosci 32:658–73.

Klein T, Proppert S, Sauer M. 2014. Eight years of single-molecule localization microscopy. Histochem Cell Biol. 141:561-75.

Leal-Ortiz S, Waites CL, Terry-Lorenzo R, Zamorano P, Gundelfinger ED, Garner CC. 2008. Piccolo modulation of Synapsin1a dynamics regulates synaptic vesicle exocytosis. J Cell Biol 181:831-46.

Leonard AS, Davare MA, Horne MC, Garner CC, Hell JW. 1998. SAP97 is associated with the alpha-Amino-3-hydroxy-5-methylisoxazole-4-propionic acid receptor GluR1 subunit. J Biol Chem 273:19518–19524.

Li D, Specht CG, Waites CL, Butler-Munro C, Leal-Ortiz S, Foote JW, Genoux D, Garner CC, Montgomery JM. 2011. SAP97 directs NMDA receptor spine targeting and synaptic plasticity. J Physiol 589:4491–4510.

Lin EI, Jeyifous O, Green WN. 2013. CASK regulates SAP97 conformation and its interactions with AMPA and NMDA receptors. J Neurosci 33:12067–12076.

Lissin D V, Gomperts SN, Carroll RC, Christine CW, Kalman D, Kitamura M, Hardy S, Nicoll RA, Malenka RC, von Zastrow M. 1998. Activity differentially regulates the surface expression of synaptic AMPA and NMDA glutamate receptors. Proc Natl Acad Sci 95:7097–7102.

Liu M, Lewis LD, Shi R, Brown EN, Xu W. 2014. Differential requirement for NMDAR activity in SAP97β-mediated regulation of the number and strength of glutamatergic AMPAR-containing synapses. J Neurophysiol 111:648–658.

Lois C, Hong EJ, Pease S, Brown EJ, Baltimore D. 2002. Germline transmission and tissue-specific expression of transgenes delivered by lentiviral vectors. Science 295:868–872.

Lüscher C, Nicoll RA, Malenka RC, Muller D. 2000. Synaptic plasticity and dynamic modulation of the postsynaptic membrane. Nat Neurosci. 3:545-50.

MacGillavry HD, Song Y, Raghavachari S, Blanpied TA. 2013. Nanoscale scaffolding domains within the postsynaptic density concentrate synaptic AMPA receptors. Neuron 78:615–622.

Makino H, Malinow R. 2009. AMPA receptor incorporation into synapses during LTP: the role of lateral movement and exocytosis. Neuron 64:381–390.

Malinow R, Mainen ZF, Hayashi Y. 2000. LTP mechanisms: From silence to four-lane traffic. Curr Opin Neurobiol 10:352–357.

Malinow R, Malenka RC. 2002. AMPA receptor trafficking and synaptic plasticity. Annu Rev Neurosci 25:103-26.

Man H-Y, Lin JW, Ju WH, Ahmadian G, Liu L, Becker LE, Sheng M, Wang YT. 2000. Regulation of AMPA receptor–mediated synaptic transmission by clathrin-dependent receptor internalization. Neuron 25:649–662.

Mauceri D, Cattabeni F, Di Luca M, Gardoni F. 2004. Calcium/calmodulin-dependent protein kinase II phosphorylation drives synapse-associated protein 97 into spines. J Biol Chem 279:23813–23821.

Mauceri D, Gardoni F, Marcello E, Di Luca M. 2007. Dual role of CaMKII-dependent SAP97 phosphorylation in mediating trafficking and insertion of NMDA receptor subunit NR2A. J Neurochem 100:1032–1046.

Montgomery JM, Pavlidis P, Madison DV. 2001. Pair recordings reveal all-silent synaptic connections and the postsynaptic expression of long-term potentiation. Neuron 29:691-701.

Montgomery JM, Zamorano PL, Garner CC. 2004. MAGUKs in synapse assembly and function: an emerging view. Cellular and Molecular Life Sciences 61:911-929.

Murthy VN, Schikorski T, Stevens CF, Zhu Y. 2001. Inactivity produces increases in neurotransmitter release and synapse size. Neuron 32:673–682.

Nair D, Hosy E, Petersen JD, Constals A, Giannone G, Choquet D, Sibarita JB. 2013. Super-resolution imaging reveals that AMPA receptors inside synapses are dynamically organized in nanodomains regulated by PSD95. J Neurosci 33:13204–13224.

Nakagawa T, Futai K, Lashuel HA, Lo I, Okamoto K, Walz T, Hayashi Y, Sheng M. 2004. Quaternary structure, protein dynamics, and synaptic function of SAP97 controlled by L27 domain interactions. Neuron 44:453–467.

Nash JE, Appleby VJ, Corrêa SL, Wu H, Fitzjohn SM, Garner CC, Collingridge GL, Molnár E. 2010. Disruption of the interaction between myosin VI and SAP97 is associated with a reduction in the number of AMPARs at hippocampal synapses. J Neurochem 112:677–690.

Niethammer M, Kim E, Sheng M. 1996. Interaction between the C terminus of NMDA receptor subunits and multiple members of the PSD-95 family of membrane-associated guanylate kinases. J Neurosci 16:2157–2163.

Oh MC, Derkach VA, Guire ES, Soderling TR. 2006. Extrasynaptic membrane trafficking regulated by GluR1 serine 845 phosphorylation primes AMPA receptors for long-term potentiation. J Biol Chem 281:752-758.

Opazo P, Labrecque S, Tigaret CM, Frouin A, Wiseman PW, De Koninck P, Choquet D. 2010. CaMKII Triggers the Diffusional Trapping of Surface AMPARs through Phosphorylation of Stargazin. Neuron 67:239-252.

Osterweil E, Wells DG, Mooseker MS. 2005. A role for myosin VI in postsynaptic structure and glutamate receptor endocytosis. J Cell Biol 168:329–338.

Park M, Salgado JM, Ostroff L, Helton TD, Robinson CG, Harris KM, Ehlers MD. 2006. Plasticity-induced growth of dendritic spines by exocytic trafficking from recycling endosomes. Neuron 52:817–30.

Patterson MA, Szatmari EM, Yasuda R. (2010). AMPA receptors are exocytosed in stimulated spines and adjacent dendrites in a Ras-ERK-dependent manner during long-term potentiation. Proc Natl AcadSci 107:15951–15956.

Petralia RS, Wang Y-X, Wenthold RJ. 2003. Internalization at glutamatergic synapses during development. Eur J Neurosci 18:3207–3217.

Petrini EM, Lu J, Cognet L, Lounis B, Ehlers MD, Choquet D. 2009. Endocytic trafficking and recycling maintain a pool of mobile surface AMPA receptors required for synaptic potentiation. Neuron 63:92–105.

Poglia L, Muller D, Nikonenko I. 2010. Ultrastructural modifications of spine and synapse morphology by SAP97. Hippocampus 21:990–998.

Raghavachari S, Lisman JE. 2004. Properties of quantal transmission at CA1 synapses. J Neurophysiol 92:2456–2467.

Regalado MP, Terry-Lorenzo RT, Waites CL, Garner CC, Malenka RC. 2006. Transsynaptic signaling by postsynaptic synapse-associated protein 97. J Neurosci 26:2343–2357.

Rumbaugh G, Sia G. 2003. Synapse-associated protein-97 isoform-specific regulation of surface AMPA receptors and synaptic function in cultured neurons. J Neurosci 23:4567–4576.

Rust MJ, Bates M, Zhuang X. 2006. Sub-diffraction-limit imaging by stochastic optical reconstruction microscopy (STORM). Nat Methods 3:793-5.

Sans N, Racca C, Petralia RS, Wang Y-X, McCallum J, Wenthold RJ. 2001. Synapse-associated protein 97 selectively associates with a subset of AMPA receptors early in their biosynthetic pathway. J Neurosci 21:7506–7516.

Schlüter OM, Xu W, Malenka RC. 2006. Alternative N-terminal domains of PSD-95 and SAP97 govern activity-dependent regulation of synaptic AMPA receptor function. Neuron 51:99–111.

Schneider CA, Rasband WS, Eliceiri KW. 2012. NIH Image to ImageJ: 25 years of image analysis. Nature Methods 9:671-675

Schnell E, Sizemore M, Karimzadegan S, Chen L, Bredt DS, Nicoll RA. 2002. Direct interactions between PSD-95 and stargazin control synaptic AMPA receptor number. Proc Natl Acad Sci 99:13902–13907.

Shi S-H, Hayashi Y, Esteban JA, Malinow R. 2001. Subunit-specific rules governing AMPA receptor trafficking to synapses in hippocampal pyramidal neurons. Cell 105:331–343.

Szepesi Z, Hosy E, Ruszczycki B, Bijata M, Pyskaty M, Bikbaev A, Heine M, Choquet D, Kaczmarek L, Wlodarczyk J. 2014. Synaptically released matrix metalloproteinase activity in control of structural plasticity and the cell surface distribution of GluA1-AMPA receptors. PLoS ONE 9:5.

Tanaka H, Hirano T. 2012. Visualization of subunit-specific delivery of glutamate receptors to postsynaptic membrane during hippocampal long-term potentiation. Cell Reports 1:291–298.

Tao-Cheng JH, Crocker VT, Winters CA, Azzam R, Chludzinski J, Reese TS. 2011. Trafficking of AMPA receptors at plasma membranes of hippocampal neurons. J Neurosci 31:4834–43.

Tardin C, Cognet L, Bats C, Lounis B, Choquet D. 2003. Direct imaging of lateral movements of AMPA receptors inside synapses. EMBO J 22:4656–4665.

Tokunaga M, Imamoto N, Sakata-Sogawa K. 2008. Highly inclined thin illumination enables clear single-molecule imaging in cells. Nat Methods 5:159–161.

Turrigiano G, Leslie KR, Desai NS, Rutherford LC, Nelson SB. 1998. Activity-dependent scaling of quantal amplitude in neocortical neurons. Nature 391:892–896.

van de Linde S, Endesfelder U, Mukherjee A, Schüttpelz M, Wiebusch G, Wolter S, Heilemann M, Sauer M. 2009. Multicolor photoswitching microscopy for subdiffraction-resolution fluorescence imaging. Photochem Photobiol Sci 8:465-9.

Vitureira N, Goda Y. 2013. Cell biology in neuroscience: the interplay between Hebbian and homeostatic synaptic plasticity. J Cell Biol 203:175-86.

Waites CL, Specht CG, Hartel K, Leal-Ortiz S, Genoux D, Li D, Drisdel RC, Jeyifous O, Cheyne JE, Green WN, Montgomery JM, Garner CC. 2009. Synaptic SAP97 isoforms regulate AMPA receptor dynamics and access to presynaptic glutamate. J Neurosci 29:4332–4345.

Wang Z, Edwards JG, Riley N, Provance DW, Li X, Davison IG, Ikebe M, Mercer JA, Kauer JA, Ehlers MD. 2009. Mysoin Vb mobilizes recycling endosomes and AMPA receptors for postsynaptic plasticity. Cell 135:535–548.

Wu H, Nash JE, Zamorano P, Garner CC. 2002. Interaction of SAP97 with minus-end-directed actin motor myosin VI. Implications for AMPA receptor trafficking. J Biol Chem 277:30928–30934.

Yudowski GA. 2007. Real-time imaging of discrete exocytic events mediating surface delivery of AMPA receptors. J Neurosci 27:11112–11121.

Zhang L, Hsu FC, Mojsilovic-Petrovic J, Jablonski AM, Zhai J, Coulter DA, Kalb R. 2015. Structure–function analysis of SAP97, a modular scaffolding protein that drives dendrite growth. Mol Cell Neurosci 65:31–44.

Zheng C-Y, Seabold GK, Horak M, Petralia RS. 2011. MAGUKs, synaptic development, and synaptic plasticity. Neuroscientist 17:493–512.

Zhou W, Zhang L, Guoxiang X, Mojsilovic-Petrovic J, Takamiya K, Sattler R, Huganir RL, Kalb R. 2008. GluR1 controls dendrite growth through its binding partner, SAP97. J Neurosci 28:10220–10233.

Acknowledgments:

The authors wish to thank members of the Montgomery and Soeller labs for helpful discussion. This work was supported by the Auckland Medical Research Foundation and The University of Auckland. The authors have no conflict of interest to declare.

Figure Legends

Figure 1: Relative location of surface Flag-GluA1 in SAP97 transfected neurons. Neurons were co-transfected with Flag-GluA1 and (A) αSAP97, (B) βSAP97, (C) eGFP and immunolabelled with postsynaptic Homer (red) to label excitatory PSDs, and surface Flag (cyan) to label exogenous GluA1-containing AMPA receptors. Dendritic outline from widefield GFP immunolabelling is shown with white solid line. Below: Magnified images from boxed regions (white dashed squares) showing example "side" and "face" views of Homer (PSD) and GluA1 clusters. White arrowheads indicate example extrasynaptic receptor clusters. (D): Total amount of surface Flag-GluA1 labelling per square micron of dendrite. (E): Number of discrete Flag-GluA1 clusters per square micron of dendritic membrane. Bar graphs show mean ± SEM. Scale bar = 1μm (top), 500 nm (zoom images).

Figure 2: Quantification of synaptic, perisynaptic and extrasynaptic surface GluA1 clusters in SAP97 transfected neurons. (A). The fraction of Flag-GluA1 labelling located at synaptic and extrasynaptic sites. (B) Boxplot illustrating the size of synaptic Flag-GluA1 clusters. (C) Line graph illustrating the location of extrasynaptic Flag-GluA1 immunolabelling relative to the edge of the PSD. (D) The fraction of perisynaptic Flag-GluR1 labelling, i.e. labelling located within 100 μm of the PSD edge. (E) Boxplot illustrating the size of extrasynaptic Flag-GluA1 clusters. * indicates statistical difference compared to eGFP controls (ANOVA or K-W test: $p < 0.05$, n = 17, 18, 24 images, for αSAP97, βSAP97, and eGFP respectively). Bar graphs show mean ± SEM.

Figure 3: Density of Homer and Flag-GluA1 labelling at SAP97 and Flag-GluA1 co-expressing postsynaptic clusters. Neurons were transfected with Flag-GluA1 and (A) αSAP97, (B) βSAP97, (C) eGFP and immunolabelled with postsynaptic Homer (red) to label excitatory PSDs, and surface Flag (cyan) to label exogenous GluA1-containing AMPA receptors. (D) Boxplot showing the size spread of postsynaptic Homer clusters. (E, F): The density of Flag-GluA1 and Homer labelling at PSDs. * indicates statistical difference compared to eGFP controls (ANOVA or K-W test: $p < 0.05$; n = 392/18, 310/18, 323/24 clusters/images, for αSAP97, βSAP97, and eGFP respectively). Bar graphs show mean ± SEM. Scale bar = 200 nm.

Figure 4: Presynaptic Bassoon and postsynaptic Homer in SAP97-transfected synapses. Neurons were transfected with (A) αSAP97, (B) βSAP97, (C) eGFP, immunolabelled with antibodies against postsynaptic Homer (red) and presynaptic Bassoon (blue) and imaged with dSTORM. (D): Boxplot showing size spread of presynaptic Bassoon clusters. * indicates statistical

difference compared to eGFP controls (K-W test: $p < 0.05$; n = 277/23, 202/17, 141/16 synapses/images for αSAP97, βSAP97, and eGFP respectively). (E): Left: Percentage of SAP97 puncta that co-localise with presynaptic FM4-64 puncta (mean ± SEM). * $p < 0.05$, students t-test between αSAP97 and βSAP97. Right: Example confocal images of αSAP97 (left, green) and βSAP97 (right, green) with FM4-64 labelling (red) in hippocampal neurons. Arrowheads indicate SAP97 puncta that co-localise with FM4-64, with co-localisation occurring significantly more frequently in αSAP97-expressing neurons. Scale bar: 5 μm.

Figure 5: Morphology of SAP97-expressing neurons. Neurons were transfected with (A) αSAP97, (B) βSAP97, (C) eGFP and imaged with confocal microscopy. (D): Total area of the dendritic tree, excluding the soma. (E): Proportion of dendritic spines classified as filopodia (black bars) or mushroom-shaped spines (gray bars) at 14 DIV. Inset: example filopodium (top) and mushroom spine (bottom). (F): Proportion of dendritic spines classified as filopodia (black bars) or mushroom-shaped spines (gray bars) at 21 DIV. * indicates statistical difference ($p < 0.001$). Bar graphs show mean ± SEM. Scale bar = 10μm (A – C) and 1μm (E).

Figure 6: AMPA receptor expression on SAP97-expressing filopodia. Neurons were co-transfected with Flag-GluA1 and (A) αSAP97, (B) βSAP97, (C) eGFP and immunolabelled with surface Flag (cyan) to label exogenous GluA1-containing AMPA receptors. (D): Surface area of filopodia occupied with Flag-GluA1 labelling. n = 17/11, 28/18, 16/11 filopodia/images. Scale bar = 500nm. * indicates statistical difference compared to eGFP controls (ANOVA: $p < 0.05$; n = 16, 32, 36 images, for αSAP97, βSAP97, and eGFP respectively).

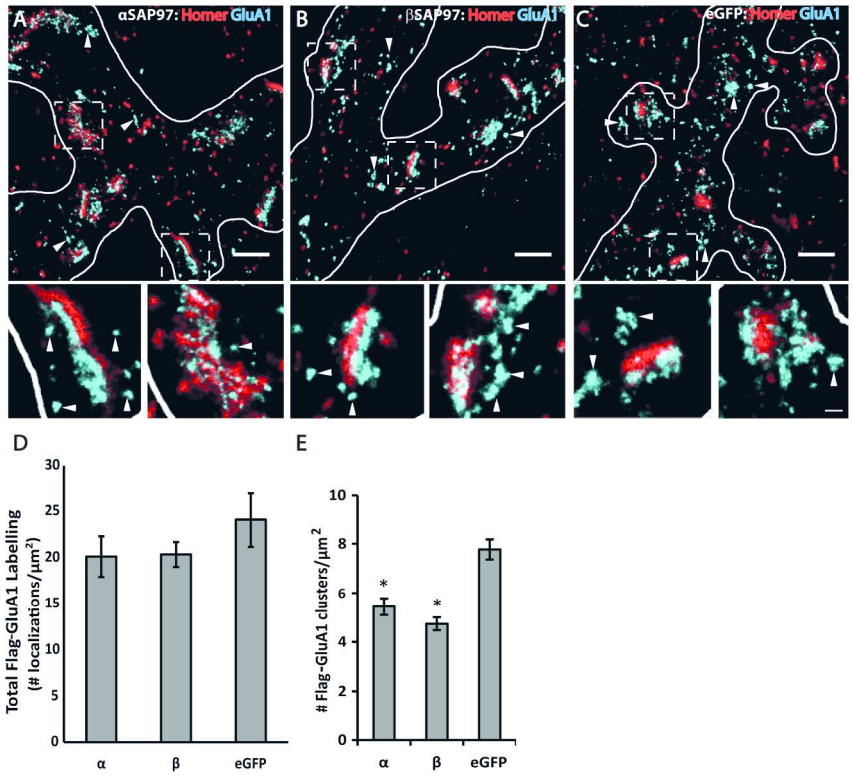

Figure 1

218x176mm (300 x 300 DPI)

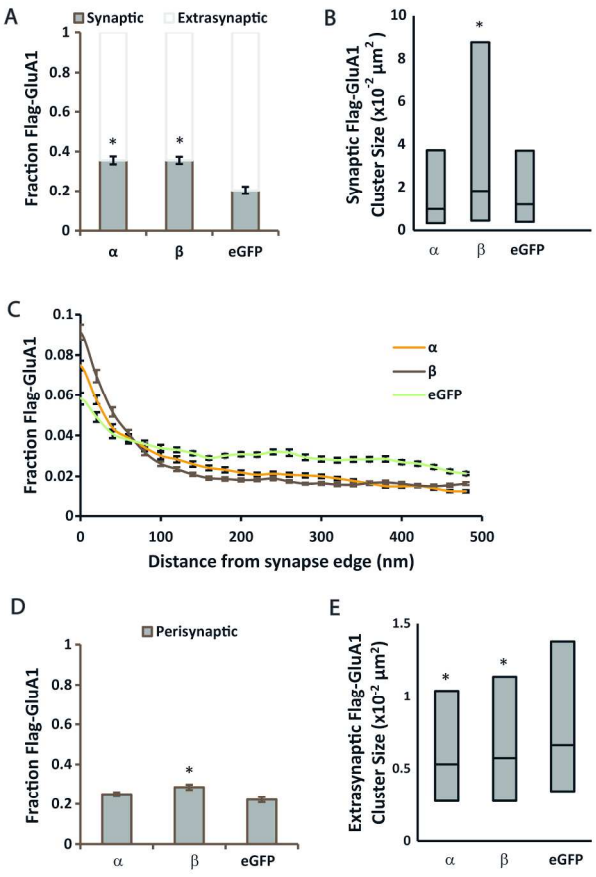

Figure 2

219x197mm (300 x 300 DPI)

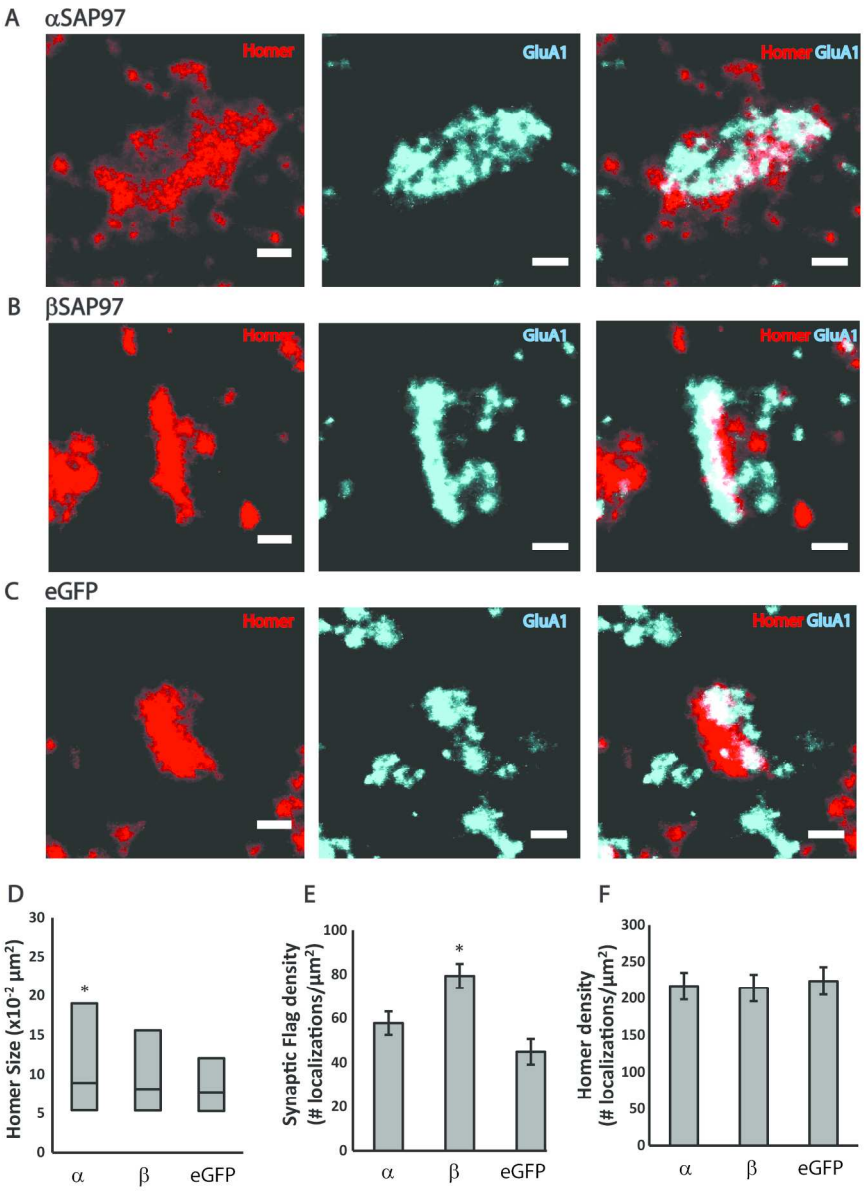

Figure 3

196x240mm (300 x 300 DPI)

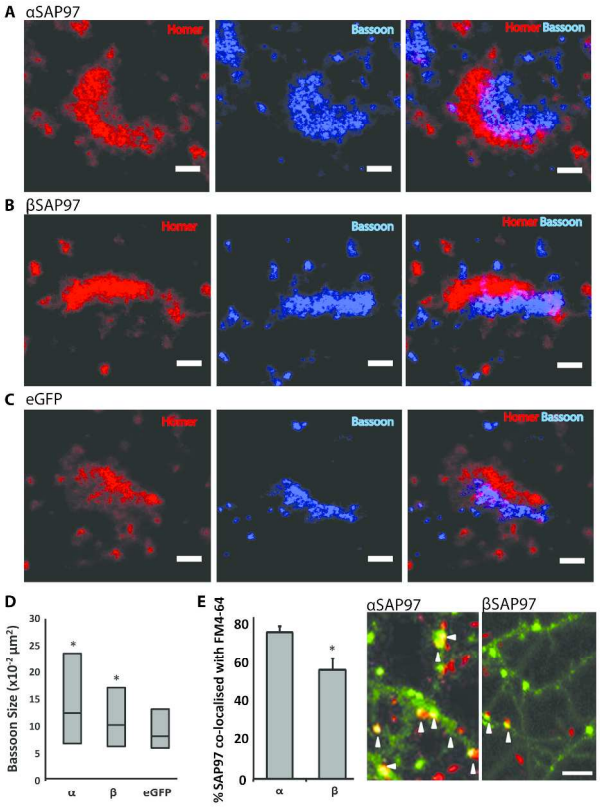

Figure 4

215x347mm (300 x 300 DPI)

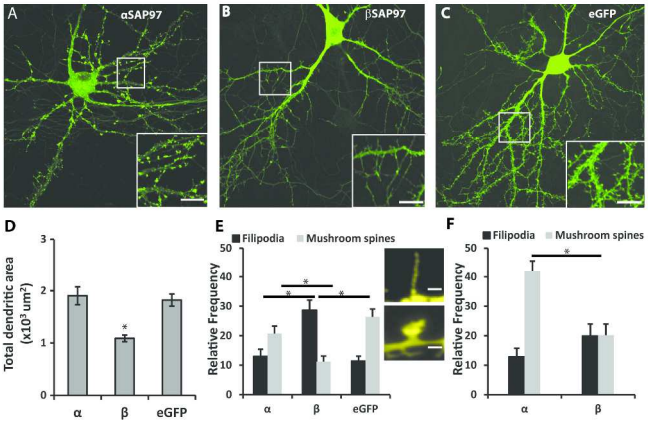

Figure 5

223x353mm (300 x 300 DPI)

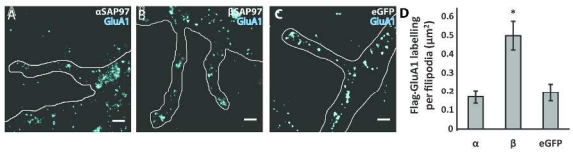

Figure 6

356x325mm (300 x 300 DPI)